Nanoelectronics and Its New Materials – A NEW ERA OF NANOSCIENCE

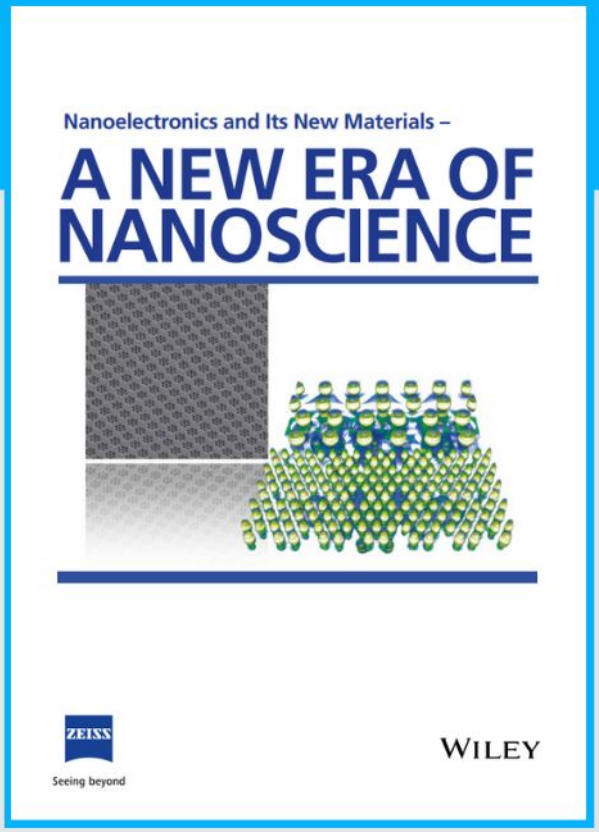

Discover the recent advances in electronics research and fundamental nanoscience.

Nanotechnology has become the driving force behind breakthroughs in engineering, materials science, physics, chemistry, and biological sciences. In this compendium, we delve into a wide range of novel applications that highlight recent advances in electronics research and fundamental nanoscience. From surface analysis and defect detection to tailored optical functionality and transparent nanowire electrodes, this eBook covers key topics that will revolutionize the future of electronics.

To get your hands on this valuable resource and unleash the power of nanotechnology, simply download the eBook now. Stay ahead of the curve and embrace the future of electronics with nanoscience as your guide.

ZEISS

Seeing beyond

WILEY

ADVANCED FUNCTIONAL MATERIALS
www.afm-journal.de

Solvent-Free Electrolyte for High-Temperature Rechargeable Lithium Metal Batteries

An L Phan, Chamithri Jayawardana, Phung ML Le, Jiaxun Zhang, Bo Nan, Weiran Zhang, Brett L Lucht, Singyuk Hou, and Chunsheng Wang**

The formation of lithiophobic inorganic solid electrolyte interphase (SEI) on Li anode and cathode electrolyte interphase (CEI) on the cathode is beneficial for high-voltage Li metal batteries. However, in most liquid electrolytes, the decomposition of organic solvents inevitably forms organic components in the SEI and CEI. In addition, organic solvents often pose substantial safety risks due to their high volatility and flammability. Herein, an organic-solvent-free eutectic electrolyte based on low-melting alkali perfluorinated-sulfonimide salts is reported. The exclusive anion reduction on Li anode surface results in an inorganic, LiF-rich SEI with high capability to suppress Li dendrite, as evidenced by the high Li plating/stripping CE of 99.4% at 0.5 mA cm^{-2} and 1.0 mAh cm^{-2}, and 200-cycle lifespan of full $LiNi_{0.8}Co_{0.15}Al_{0.05}O_2$ (2.0 mAh cm^{-2}) || Li (20 µm) cells at 80 °C. The proposed eutectic electrolyte is promising for ultrasafe and high-energy Li metal batteries.

1. Introduction

Lithium (Li) metal is the ultimate anode for rechargeable batteries. Its high specific capacity (3860 mAh g^{-1}) and low voltage (−3.04 V vs standard hydrogen electrode) warrant optimal cell energy density. However, the adoption of Li metal anode is currently plagued by Li dendrite growth during charge/discharge cycles. Organic liquid electrolytes readily react with Li forming mosaic solid-electrolyte interphases (SEIs) with high organic contents and high lithiophilicity (i.e., low interfacial energy against Li), which energetically favor the Li vertical growth into the SEI as dendrite over the planar growth along Li–SEI interface. Due to high reactivity, Li dendrites are well known not only to damage the cell cycle life via continuous consumption of both Li and electrolytes; but also, to cause severe safety issues.[1] To reverse this unwanted pattern, the SEI composition is to be tailored to maximize the SEI interfacial energy against the electrodes. Organic components are generally lithiophilic and thus should be limited while inorganic components, especially LiF, with its unmatched interfacial energy against Li and great mechanical strength,[2] need to be enriched. An effective approach to this end is to promote the reduction of inorganic salts, especially those containing labile fluorine atoms, over that of organic solvents by using either high-concentration, localized high-concentration, or fluorinated ether electrolytes.[3–8] Nonetheless, such advanced designs still rely on the use of organic solvents to maintain adequate transport properties, so the formation of organic species on Li surface could not be completely eliminated. Another intrinsic problem of organic solvents is their high flammability, which, in combination with their inability to passivate Li anode and suppress Li dendrites, can lead to serious fiery incidents.[9] Banishing the solvents from the electrolyte formula appears to be a promising solution for the abovementioned challenges.

Without a solvent, the salts need to be in the molten state to enable sufficient ion conduction and electrode wetting. The prohibitively high melting point of most Li salts, however, disqualifies their use as a single molten salt electrolyte for Li-based batteries due to limited applicability as well as complications concerning inferior stability and workability of other cell components at extreme conditions.[10] The most well-known strategy to lower the salt melting points relies on the eutectic concept. In the ideal case, mixing two or more components

A. L Phan, J. Zhang, S. Hou, C. Wang
Department of Chemical and Biomolecular Engineering
University of Maryland
College Park, MD 20742, USA
E-mail: shou12@umd.edu; cswang@umd.edu

C. Jayawardana, B. L Lucht
Department of Chemistry
University of Rhode Island
Kingston, RI 02881, USA

P. M. Le
Energy & Environment Directorate
Pacific Northwest National Laboratory
Richland, WA 99354, USA

B. Nan, C. Wang
Department of Chemistry and Biochemistry
University of Maryland
College Park, MD 20742, USA

W. Zhang
Department of Materials Science and Engineering
University of Maryland
College Park, MD 20742, USA

The ORCID identification number(s) for the author(s) of this article can be found under https://doi.org/10.1002/adfm.202301177

DOI: 10.1002/adfm.202301177

that are miscible in the liquid phase but immiscible in the solid phase leads to depression in the mixture melting point, as the introduction of mixing entropy lowers the free energy of (i.e., stabilizes) the liquid phase. This stabilization effect could be enhanced if there are attractive interactions between components, which help to lower the liquid phase enthalpy.[11] Based on the principle described above, Li-conductive mixtures with reasonably low melting points (typically below 100 °C) have been prepared from perfluorinated-sulfonimide salts of Li and other alkali metals and investigated as nonflammable electrolytes for Li-ion batteries.[10,12–16] Unlike dilute solutions of alkali metal bis(trifluoromethanesulfonyl)imide (TFSI) and bis(fluorosulfonyl)imide (FSI), these molten salt electrolytes can passivate the aluminum current collector at up to 5.0 V.[10,14] Their electrochemical performance in low-voltage $LiFePO_4$ (LFP) || graphite Li-ion batteries has also been demonstrated.[10,12–14] However, no improvement compared to the conventional electrolytes was observed, because the organic-inorganic mixed SEI can fully support the low-voltage low-expansion materials. In addition, the reported data are largely limited to low active material loading (below 0.5 mAh cm^{-2}), presumably due to low Li concentration resulting in mediocre Li transference number (t_{Li}) of the electrolytes (the highest t_{Li} reported to date is 0.3[14]). In combination with the unfavorable viscosity and ionic mobility typically observed for molten salts at the temperature range of interest (i.e., below 100 °C), such t_{Li} values render the systems prone to concentration polarization even under moderate working current densities and capacities. Local solidification and significant conductivity drop might happen as a result, eventually leading to cell failure.

Interestingly, the plating/stripping behavior of Li metal in inorganic molten salts has never been studied, to the best of our knowledge, although their organic-solvent-free characteristic is beneficial for high-voltage Li metal batteries. It is worth noting that due to the negligibly low vapor pressure of molten salt electrolytes, their use could shift upward the battery working temperature limits, promising applicability to non-ambient systems, such as those for downhole use in the oil and gas industry.[17,18] Specific applications in military, aerospace, and most importantly, electric vehicle industries may also prefer high-temperature batteries with high safety, as they help simplify the thermal management problem, essentially reducing the cost, weight, and other complications of extra cooling systems.[18–20] In fact, previous studies indicated that high temperatures have a positive impact on Li deposition morphology and cycling efficiency,[21–23] suggesting good prospects for the currently underexplored field of high-temperature rechargeable Li metal batteries.

In this study, we report a molten salt mixture (45 wt.% LiFSI, 45 wt.% CsTFSI, 10 wt.% LiTFSI, denoted as LCsL10) as a safe electrolyte for high-temperature Li metal batteries. In the absence of organic solvents, the SEI on Li surface is solely derived from perfluorinated-sulfonimide anions, thus rich in robust and stable LiF. Such an SEI effectively accommodates large volume change of Li anode during cycling and inhibits Li dendrites as well as unwanted side reactions, even at elevated temperatures. It is noteworthy that LCsL10 has a higher Li content and thus a higher Li transference number (t_{Li} = 0.52 at 80 °C) compared to previously reported molten salt electrolytes, so it is less prone to concentration polarization during charge/discharge, promising better workability at practical currents and areal capacities. As a proof of concept, we demonstrated that at 80 °C, LCsL10 supports an average Li plating/stripping Coulombic efficiency (Li CE) of 99.4% over more than 150 cycles at 0.5 mA cm^{-2} and 1.0 mAh cm^{-2}, and enables $LiNi_{0.8}Co_{0.15}Al_{0.05}O_2$ (NCA) || Li full cell (2.0 mAh cm^{-2}, N/P = 2) to achieve a cycle life of 200. This is the first report on a molten salt electrolyte for Li metal batteries using nickel-rich layered oxide cathodes.

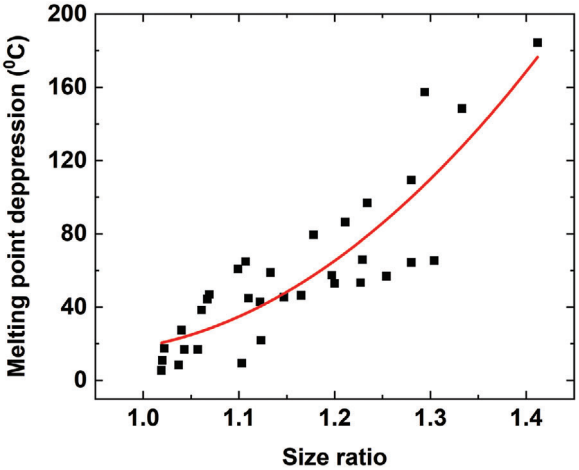

Figure 1. Correlation between melting point depression and "size" ratio of previously reported binary alkali metal salt mixtures. The data points (■) were adopted from literatures[15,16,26,27] and fitted using a 2nd order polynomial function (red curve). The "size" of a component is defined as the sum of its cation and anion radii. Details are provided in Table S1 (Supporting Information).

2. Results and Discussion

2.1. Composition Design and Physical Properties

Molten salt electrolytes, due to their solvent-free nature, usually have melting points well above room temperature. Therefore, systems with low melting points are desirable as they offer wider working temperature range and possibly, better transport properties (viscosity and conductivity) at a given temperature. An analysis of reported binary mixtures of alkali metal salts (**Figure 1**; Table S1, Supporting Information) reveals a positive correlation between the depression in melting point (i.e., the temperature difference between the average of the component melting points and the actual eutectic temperature) and the size ratio of the two salt components. The size of a component is defined as the sum of its cation and anion radii. Despite the presence of local inconsistencies, which are caused by various factors, either extrinsic (discrepancies in the criteria used to determine the melting/eutectic temperatures in different literatures) or intrinsic (the formation of binary compounds and their relative stability affecting the system thermal behavior), the general trend is clearly visible. To achieve a low eutectic temperature, the salts should have low melting points and large differences in size. Accordingly, we are interested in the LiFSI – CsTFSI system because LiFSI and CsTFSI have low melting points of 140 and 122 °C,

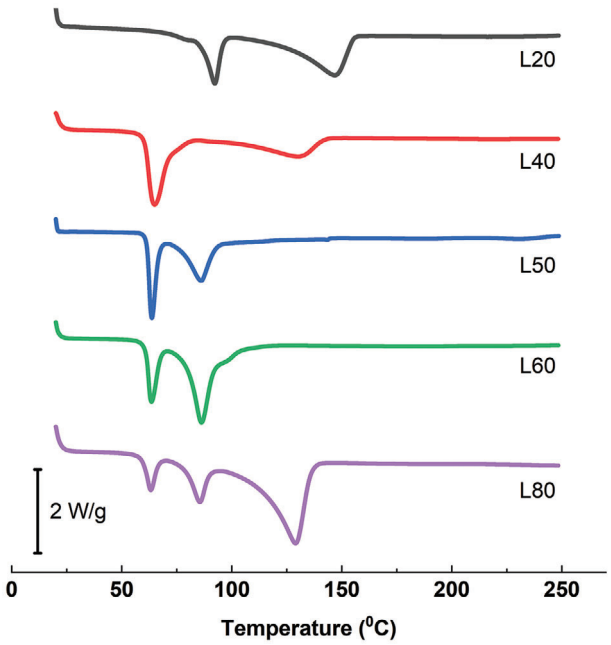

Figure 2. Thermal behavior of x wt.% LiFSI – (100-x) wt.% CsTFSI. DSC measurements were carried out under Ar flow at the heating rate of 10 °C min^{-1}.

respectively, and a larger size ratio (1.395) compared to the published same-anion systems (Table S1, Supporting Information). In addition, FSI – TFSI multi-anion ionic liquids have been evidenced to inherit the advantages of both FSI and TFSI anions.[24] They show better conductivity compared to systems based solely on TFSI anion, as well as better oxidative and thermal stability compared to those based solely on FSI anion.[25] Thus, LiFSI – CsTFSI is expected to be more well-rounded as an electrolyte than previously reported molten salts.

Thermal properties of LiFSI – CsTFSI mixtures at various LiFSI weight percentages between 20 and 80 wt.% LiFSI (denoted as L20 to L80) were investigated by differential scanning calorimetry (DSC) (**Figure 2**). In general, all compositions demonstrated good thermal stability up to 250 °C, as no exothermic peak was observed. Mixtures from L40 to L80 all showed the first melting peak at around 58 °C while L20 did not melt until 85 °C. The variation in the onset temperature of the first melting peak suggests deviations from regular binary systems. Nevertheless, it is clear that the (lower) eutectic temperature of LiFSI – CsTFSI system is 58 °C and is indeed lower than that of LiFSI – CsFSI system (62 °C).[15] Although the reduction in melting point is smaller than expected (which might be due to non-regular interactions between LiFSI and CsTFSI), it is qualitatively consistent with our hypothesis about the relationship between melting point depression of binary systems and components' size difference. A detailed analysis about the phase diagram of LiFSI – CsTFSI system is beyond the scope of this study and may be a subject for future research.

Conductivity is another essential attribute that needs optimization as it has direct impact on electrochemical performance of the electrolyte. A comparison in ion conduction behavior between various compositions of interest is shown in **Figure 3**. Among LiFSI – CsTFSI binary mixtures, L50 has the lowest activation energy for ion transport. To further enhance the electrolyte thermal and transport properties, 10 wt.%. LiTFSI was added to L50 to form LCsL10 (45 wt.% LiFSI, 45 wt.% CsTFSI, and 10 wt.% LiTFSI). LiTFSI was chosen because the use of a Li salt would avoid compromise in the Li mole fraction and the Li transference number, while the good thermal stability of TFSI anion is beneficial for high-temperature applications. As mentioned above, the introduction of a new component results in additional entropy (i.e., degree of disorder) for the system, which might facilitate ion transport. Indeed, LCsL10 maintains high thermal stability (up to 250 °C) and shows a strong resistance toward crystallization (Figure S1, Supporting Information). More importantly, LCsL10 offers improved conductivity at temperatures below 90 °C (Figure 3a) and shows lower activation energy for ion transport (Figure 3b) compared to all the binary mixtures. Although L60 shows better conductivity at temperatures above 90 °C, it is not favored over LCsL10 because competent conductivities at temperatures closer to ambient is more relevant to cell performance and applicability. Higher LiTFSI contents were not used because it was found that LCsL20 (40 wt.% LiFSI, 40 wt.% CsTFSI, and 20 wt.% LiTFSI) was barely conductive at 80 °C (0.072 mS cm^{-1}), presumably due to the high melting point of LiTFSI (234 °C).

It should be noted that the total conductivity does not necessarily reflect the individual transport rate of Li^+ ion, which governs the Li distribution throughout the electrolyte during cycling and is particularly important for Li-based systems. Therefore, we also measured the Li transference numbers using the method developed by Bruce et al.[28] (Figure 3c; Figure S2, Supporting Information). At 80 °C, the actual Li conductivity peaks at LCsL10 due to a good balance between total conductivity (0.45 mS cm^{-1}) and Li transference number (0.52), so LCsL10 was selected as our model molten salt electrolyte and used for further investigations.

2.2. Li Plating/Stripping in LCsL10

Although the standard potential of Cs^+/Cs is slightly more positive than that of Li^+/Li, previous works have reported that in Li_xCs_yTFSI and Li_xCs_yFSI molten salts, Li deposition can occur without interference from Cs^+ cation.[10,29] This is because standard potential values are given for 1.0 M aqueous solutions, where the redox properties of ionic species are heavily affected by their hydration shells, thus not necessarily applicable in solvent-free conditions such as molten salts. As expected, after 20 h of electrochemical plating at 0.5 mA cm^{-2} on Cu foil in LCsL10 electrolyte, no Cs metal could be detected by X-ray diffraction (Figure S3, Supporting Information).

The reversibility of Li plating/stripping at 80 °C in LCsL10 was investigated using coin-type Cu || Li cells, and compared to the performance of the conventional electrolyte (1.0 M $LiPF_6$ in ethylene carbonate (EC): dimethyl carbonate (DMC) 1:1 vol., denoted as EC-DMC), and an electrolyte for elevated-temperature Li metal batteries (0.8 M LiTFSI + 0.2 M lithium difluoro(oxalato)borate (LiDFOB) + 0.01 M $LiPF_6$ in EC: propylene carbonate (PC) 1:1 vol., denoted as EC-PC).[30] As shown in **Figure 4**, both EC-DMC and EC-PC at 80 °C demonstrated a limited capability to stabilize Li metal anode, as evidenced by the inferior Li CE and cycle life, although their high conductivity resulted in small

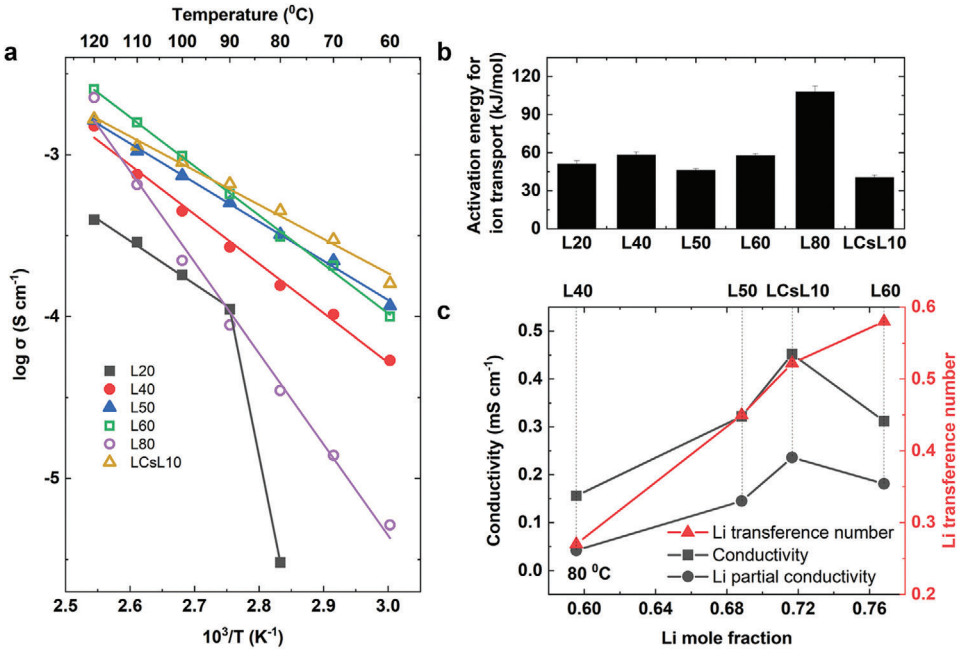

Figure 3. Conductivities of x wt.% LiFSI – (100-x) wt.% CsTFSI and LCsL10. a) Arrhenius plots of specific conductivity. b) Activation energies for ion transport. c) Li transference number and Li partial conductivity at 80 °C.

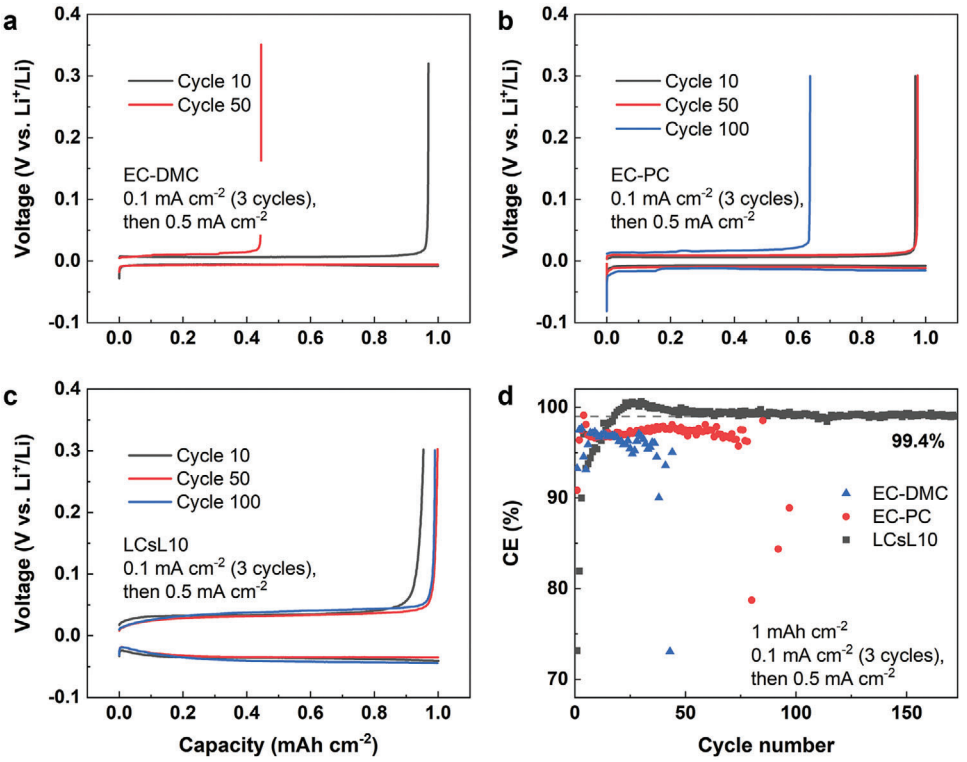

Figure 4. Electrochemical performance of Cu || Li cells at 80 °C (0.5 mA cm^{-2}, 1.0 mAh cm^{-2}). a–c) Voltage profile of the cells cycled in (a) EC-DMC, (b) EC-PC, (c) LCsL10. d) Long-cycle CE comparison.

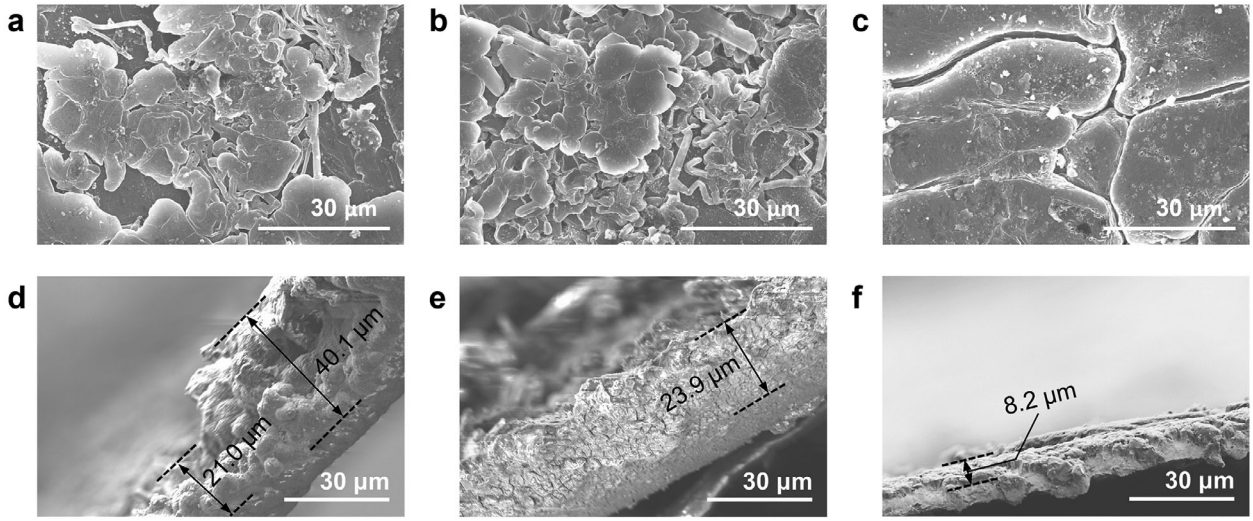

Figure 5. Morphologies of Li deposited on Cu foil in different electrolytes. a–c) Top view and d–f) cross-sectional view of Li deposited in a,d) EC-DMC, b,e) EC-PC, and c,f) LCsL10. Cu || Li cells were cycled at 0.5 mA cm^{-2}, 1.0 mAh cm^{-2}, and 80 °C. SEM images were taken after 50 cycles.

plating/stripping overpotentials. In contrast, the molten salt electrolyte allowed stable Li plating/stripping at 0.5 mA cm^{-2} and 1.0 mAh cm^{-2} with a high average Li CE of 99.4% over more than 150 cycles. At 1.0 mA cm^{-2}, the Li CE could still be maintained at 99.3% (Figure S4, Supporting Information).

To better understand the underlying reasons for such a significant difference in Li compatibility, the Li layers deposited onto Cu foils in all three electrolytes were collected and studied in terms of their morphology (by Scanning Electron Microscopy (SEM), **Figure 5**) as well as their SEI composition (by X-ray Photoelectron Spectroscopy (XPS), **Figure 6**; Figures S5 and S6, Supporting Information). As expected, the Li plated in EC-DMC was highly nonuniform, porous, and dendritic (Figure 5a,d). The EC-PC electrolyte enabled a slightly denser Li deposition, but the presence of Li dendrites and small Li flakes was still obvious as early as after 50 cycles (Figure 5b,e). The mutual problem of both electrolytes is the high reactivity of the organic solvents, which not only enriches the SEI with detrimental organic species, but also interferes with the complete anion reduction into favorable components (e.g., LiF and Li_2O[2,3,22]), resulting in a mosaic/multicomponent and shaky SEI. Indeed, XPS results revealed that the SEIs derived from EC-DMC (Figure 6a,d) and EC-PC (Figure 6b,e) are low in LiF and Li_2O, in comparison to "organic/polymeric" and "other inorganic" components. While "organic/polymeric" components are well known to facilitate Li dendrite growth, "other inorganic" components may also undermine the SEI integrity during long cycles at an elevated temperature due to the gradual but continuous evolutions of metastable compounds (e.g., $LiP_xF_yO_z$, Li_2CO_3, Li_2SO_x). The high surface area of Li dendrites, in combination with the compromised SEI stability and temperature-accelerated side reaction kinetics, eventually led to tremendous Li CE drops in both carbonate-based electrolytes. Interestingly, EC-DMC actually allowed less dendritic and more reversible Li deposition at 80 °C compared to those usually observed in 1.0 M $LiPF_6$ in nonfluorinated organic carbonates at room temperatures.[31,32] The difference is at least partially attributable to a more fully reduced and more LiF-rich SEI formed at high temperature, evidenced by a lower C/F atomic ratio (Figure S6a, Supporting Information), weaker C–O and C=O peaks, as well as the presence of low-binding-energy species (C–Li and RO–Li) (Figure 6a). Similarly, the slightly better performance of EC-PC compared to EC-DMC might be related to the higher Li_2O and lower organic content of its SEI (Figure 6d,e).

In sharp contrast, Li deposited in LCsL10 was dense and flat with larger particle size (tens of microns) (Figure 5c,f). Without the interruption from organic solvents, the anion reduction on Li metal was more thorough (consistent with the longer initial CE-climbing process), leading to the formation of an SEI rich in lithiophobic LiF. Indeed, apart from the outermost layer (sputtering time of 0 s), which is very likely contaminated by tetrahydrofuran (THF) during sample preparation and/or by the air during transfer from the glovebox to the XPS chamber, LCsL10-derived SEI showed a rather limited amount of non-LiF inorganic components and almost no organic/polymeric content (Figure 6c,f). The resulting high lithiophobicity of the SEI effectively promotes planar over vertical Li growth, resulting in a flat and dendrite-free morphology. At the same time, it helps direct the deposited Li to grow into larger particles (to minimize the unfavorable Li-SEI contact), probably through an increase in the energy barrier/critical size for Li nucleation[33] and an according decrease in the number of Li nuclei. The low electronic conductivity and good mechanical stability of LiF also help suppress Li dendrites and their reactivity as well as maintain the Li particle integrity throughout cycling.[2,31,34–36] Besides, the presence of Cs^+ ions in the electrolyte and the resulting electrostatic shielding effect[37] certainly play a role in facilitating the 2D Li growth in LCsL10. In brief, the favorable morphology and SEI of Li deposited in LCsL10 are consistent with LCsL10 superior Li CE (Figure 4d), well confirming our design principles.

2.3. $LiNi_{0.8}Co_{0.15}Al_{0.05}O_2$ (NCA) || Li Full Cell Performance in LCsL10

Along with the capability to support safe and reversible Li plating/stripping, high resistance toward oxidation is a critical

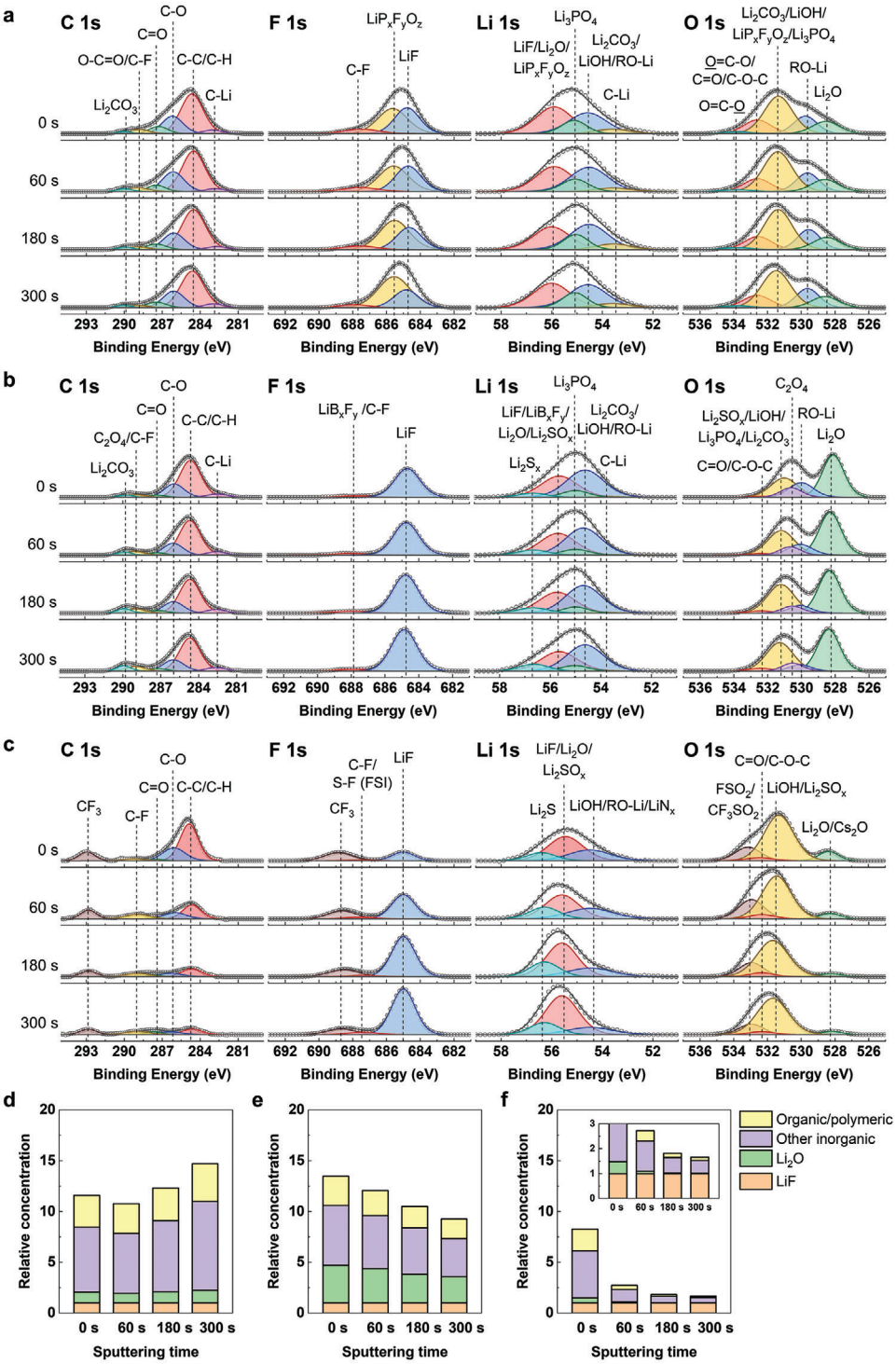

Figure 6. Surface characterization of Li deposited in different electrolytes. a–c) High-resolution C 1s, F 1s, Li 1s, and O 1s XPS spectra; and d–f) SEI relative compositions for Li deposited in a,d) EC-DMC, b,e) EC-PC, and c,f) LCsL10. High-resolution XPS spectra for other elements are provided in Figure S5 (Supporting Information). The data were collected at various depths, characterized by the sputtering time. Cu || Li cells underwent 50 cycles at 0.5 mA cm^{-2}, 1.0 mAh cm^{-2}, and 80 °C before characterization. The concentration of "Organic/polymeric" components in the SEI was characterized by the C 1s peak(s) excluding that of Li_2CO_3. "Other inorganic" concentration was calculated by subtracting LiF (F 1s), Li_2O (O 1s), RO-Li (O 1s), and C-Li (Li 1s) from the total Li 1s peak(s). All peak areas were normalized to the corresponding relative sensitivity factors (R.S.F, Table S2, Supporting Information) during calculations, then to the LiF peak areas to give the relative concentrations.

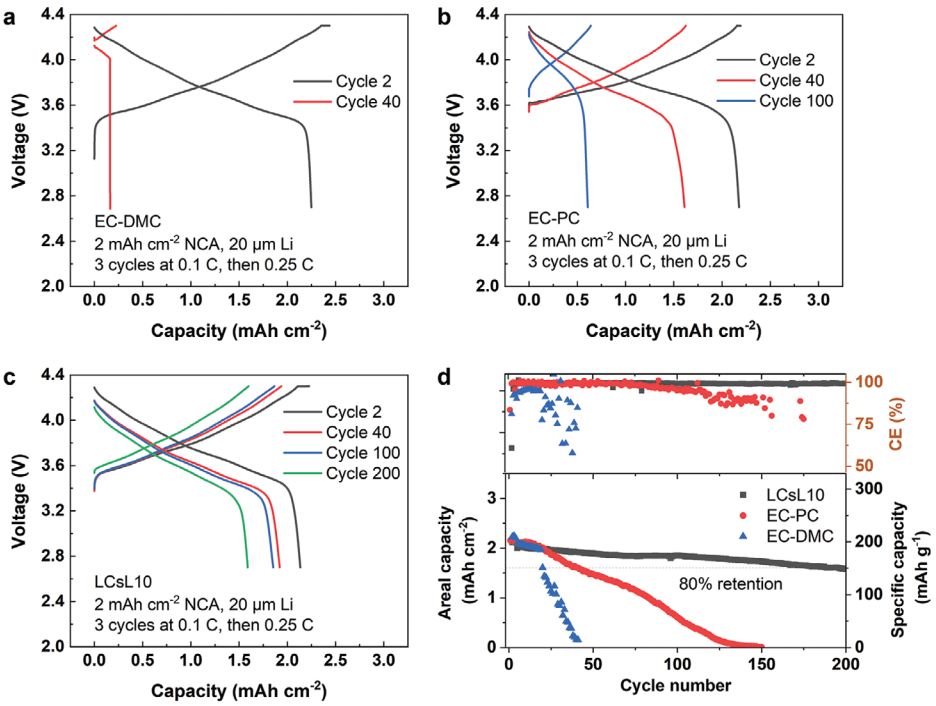

Figure 7. Electrochemical performance of full NCA (2.0 mAh cm^{-2}) || 20 μm Li cells at 80 °C. a–c) Charge–discharge curves of the cells cycled in (a) EC-DMC, (b) EC-PC, and (c) LCsL10. d) Long-term cyclability comparison.

requirement for an electrolyte to support high-voltage Li metal batteries. Cyclic voltammetry (CV) and floating tests revealed that at 80 °C, the anodic stability of LCsL10 is comparable to EC-PC (≥ 4.5 V vs Li^+/Li) and better than EC-DMC (Figure S7, Supporting Information). In particular, Al current collector cycled in LCsL10 showed a small oxidation peak when first scanned to 3.9 V, but no peak was observed during the reversed scan as well as in subsequent cycles (Figure S7c, Supporting Information), indicating complete passivation after the first cycle. The good anodic stability of LCsL10 was further corroborated by the floating test, in which Al || Li cells were constantly held at 4.5 V for 50 h (Figure S7d, Supporting Information). In good agreement with the CV results, a negligible leakage current of 1 μA cm^{-2} was observed.

Cycling performance of NCA || Li full cells using NCA cathode at a practical loading (2.0 mAh cm^{-2}) and a limited Li anode (20 μm or 4.0 mAh cm^{-2}, negative/positive electrode areal capacity ratio N/P = 2) was investigated at 80 °C to give conclusive evidence on the applicability of LCsL10 electrolyte in high-temperature Li metal batteries (**Figure 7**). While the cells cycled in EC-DMC and EC-PC reached the end of their lifespan (defined as 80% capacity retention) in less than 50 cycles, LCsL10 was able to support a 200-cycle-long cell life. The poor cyclability of the reference carbonate-based electrolytes apparently came from the loss of Li inventory, as indicated by the premature voltage drops during discharge (Figure 7a,b), as well as the sudden drops in full cell CE (Figure 7d). These results are consistent with their low and unstable Li CE (Figure 4d). Besides, the poor anodic stability of EC-DMC at 80 °C (Figure S7a,d, Supporting Information) well explained its low full cell CE, even during the initial cycles when Li excess was still available, hence the faster cyclable Li depletion compared to EC-PC. On the contrary, the cell cycled in LCsL10 showed little change in voltage profile during its cycle life, apart from small overpotential increases (Figure 7c), further verifying the good electrochemical stability of LCsL10 as well as its potential as an electrolyte for high-temperature high-energy Li metal batteries.

3. Conclusion

We report a new ternary molten salt electrolyte that can form an organic-free SEI with very high LiF content on Li anode, which is highly beneficial for Li plating/stripping reversibility and, to the best of our knowledge, has not been demonstrated in nonaqueous liquid electrolytes. Smooth and dendrite-free Li deposition with large grain size was observed. Together with the electrolyte intrinsic nonflammability, they greatly relieve the safety concerns associated with dendrite-induced short circuits and thermal runaways. At 80 °C, the electrolyte could deliver the average Li plating/stripping CE of 99.4% and the anodic stability of up to 4.5 V versus Li^+/Li, allowing decent cycling (80% capacity retention after 200 cycles) of practical NCA || Li full cells (2.7–4.3 V, 2.0 mAh cm^{-2}, N/P = 2). The combination of high-temperature performance and safety of high-voltage Li metal batteries offered by our molten salt electrolyte is unprecedented.

4. Experimental Section

Materials: LiFSI (Nippon Shokubai, 99.9%), CsTFSI (Solvionic, 99.5%), $LiPF_6$ (Gotion, battery grade), LiDFOB (Sigma–Aldrich), and 1.0 M $LiPF_6$ solution in EC: DMC 1:1 vol. (Sigma–Aldrich, battery grade) were

Table 1. Electrolytes used in this study.

Name	Composition
L20	20 wt.% LiFSI + 80 wt.% CsTFSI
L40	40 wt.% LiFSI + 60 wt.% CsTFSI
L50	50 wt.% LiFSI + 50 wt.% CsTFSI
L60	60 wt.% LiFSI + 40 wt.% CsTFSI
L80	80 wt.% LiFSI + 20 wt.% CsTFSI
LCsL10	45 wt.% LiFSI + 45 wt.% CsTFSI + 10 wt.% LiTFSI
LCsL20	40 wt.% LiFSI + 40 wt.% CsTFSI + 20 wt.% LiTFSI
EC-DMC	1.0 M $LiPF_6$ in EC: DMC 1:1 vol.
EC-PC	0.8 M LiTFSI + 0.2 M LiDFOB + 0.01 M $LiPF_6$ in EC: PC 1:1 vol.

used as received. EC (Sigma–Aldrich, 99%) was mixed with PC (Sigma–Aldrich, 99.7%) at 1:1 volume ratio and dried under activated molecular sieves overnight before use. LiTFSI was kindly provided by Army Research Lab. $LiNi_{0.8}Co_{0.15}Al_{0.05}O_2$ (NCA) electrodes (2.0 mAh cm^{-2}) were kindly provided by Saft America, Inc. Li chips (500 µm thick) and thin Li foil (20 µm thick, coated on Cu substrate) were purchased from China Energy Lithium Co., Ltd. The molten salt mixtures were prepared by stirring the components in an alumina crucible at 150 °C until a transparent liquid was obtained. Details on the composition of molten salt mixtures as well as the reference electrolytes are given in **Table 1**. Chemical handling and processing were all carried out in an argon-filled glove box ([O_2] and [H_2O] < 0.1 ppm).

Electrochemical Tests: All electrochemical tests were carried out at 80 °C in CR2032 coin cells. Li plating/stripping performance was tested in Cu || Li cells with one piece of electrodeposited Cu, one piece of separator (Celgard 3501), and two Li chips. Same configuration was applied for full NCA || Li cell, except that NCA electrode was used in place of Cu foil and 20 µm thick Li on Cu foil was used in place of Li chips. The amount of electrolyte was fixed at 30 mg for each cell, equivalent to 15 g $(Ah)^{-1}$. Charge–discharge tests were conducted on CT-3008 (Neware Technology) or CT3002AU (Landt Instruments) battery testing stations. All cells were allowed to rest at 80 °C for 12 h before charge–discharge tests. All Cu || Li cells underwent formation at 0.1 mA cm^{-2} in the first three cycles; the stripping cut-off was 0.3 V. For NCA || Li cells, the voltage range was 2.7–4.3 V. The cells underwent a pre-cycle (discharge at 0.05 C to 1.9 V; 1 C = 2.0 mAh cm^{-2}) and three formation cycles (0.1 C; held at 4.3 V for 5 h at the end of each charge) before the actual test (0.25 C; no constant-voltage step).

Conductivity and Li transference number measurements as well as cyclic voltammetry (CV) and floating tests were conducted on Gamry interface 1000E potentiostat (Gamry Instruments). Conductivity was measured by electrochemical impedance spectroscopy (EIS) following a reported protocol.[38] A glass microfiber filter film (Whatman GF/F) soaked in the electrolyte of interest was sandwiched between two blocking electrodes (stainless steel); its resistance was determined, then calibrated versus EC-DMC (conductivity = 10.7 mS cm^{-1} at 25 °C[39]) to back-calculate the electrolyte conductivity. The activation energies for ion transport were determined by fitting conductivities to the Arrhenius equation:

$$\log \sigma = \log \sigma_0 - \frac{E_A}{2.303RT} \tag{1}$$

Li transference number was measured in Li symmetric cells (Celgard 3501 as the separator) according to the method proposed by Bruce et al.[28] The cells were subjected to two pre-cycles (0.2 mA cm^{-2}, 0.2 mAh cm^{-2}) to stabilize the interphases before the actual test. The EIS measurements were taken with 5 mV AC perturbation, from 1 MHz to 0.05 Hz; for the potentiostatic polarization step, 10 mV bias was used. The CV and floating tests were performed on Al || Li cells (Celgard 3501 as the separator). For CV, the cells were scanned between 3.0–4.5 V at 0.5 mV s^{-1} for five cycles. For the floating test, the cells were held at 4.5 V for 50 h.

Material Characterization: Investigation of thermal behavior of the molten salts was conducted on a differential scanning calorimeter (DSC 25, TA instruments) equipped with a refrigerated cooling system (RCS 90, TA instruments). The samples were hermetically sealed in aluminum pans inside the glovebox and allowed to rest at room temperature for 4 days (unless stated otherwise) before subjected to thermal scanning at 10 °C min^{-1}.

The phase composition of the product deposited from LCsL10 was evaluated using X-ray diffraction (XRD) (D8 Advance, Bruker AXS) with Cu Kα radiation (λ = 1.5418 Å). No pretreatment was performed to the XRD sample. For other postmortem analysis, the electrodes recovered from EC-DMC, EC-PC, and LCsL10 were washed three times with 500 µL DMC, PC, and THF (Sigma–Aldrich, 99.9%), respectively, then dried under vacuum before tested. The morphologies of the Li deposits were examined by field emission scanning electron microscopy (SEM) (Hitachi SU-70, Hitachi) with an accelerating voltage of 10 kV. The SEI composition was studied by X-ray photoelectron spectroscopy (XPS) (K-alpha, Thermo Scientific) using Al Kα radiation (1486.6 eV). The X-ray spot size was 400 µm and the pass energy was 50 eV. Hydrocarbon peak (284.8 eV) was used to calibrate the binding energy values. Depth profiling was conducted using an Ar^+ ion gun (200 eV, 0°). Peak fitting was performed on CASA XPS software, using Shirley background and GL(30) peak shape. For S 2p and P 2p spectra, $2p_{3/2}$ and $2p_{1/2}$ peaks were constrained to 2:1 area ratio and same full width at half maximum (fwhm); the peak separations were 1.18 eV for S 2p and 0.86 eV for P 2p.

Supporting Information

Supporting Information is available from the Wiley Online Library or from the author.

Acknowledgements

The authors acknowledge helpful advice for electron microscopy experiments from Dr. Sz-Chian Liou at the AIMLab, Maryland NanoCenter. This work was supported by the Assistant Secretary for Energy Efficiency and Renewable Energy, Office of Vehicle Technologies of the US Department of Energy through the Advanced Battery Materials Research (BMR) Program (Battery500 Consortium Phase 2) under DOE contract No. DE-AC05-76RL01830 from the Pacific Northwest National Laboratory (PNNL).

Conflict of Interest

The authors declare no conflict of interest.

Data Availability Statement

The data that support the findings of this study are available from the corresponding author upon reasonable request.

Keywords

electrolytes, eutectic, high-temperature, Li metal batteries, molten salts

Received: April 3, 2023
Published online: May 8, 2023

[1] X.-B. Cheng, R. Zhang, C.-Z. Zhao, Q. Zhang, *Chem. Rev.* **2017**, *117*, 10403.

[2] X. Fan, X. Ji, F. Han, J. Yue, J. Chen, L. Chen, T. Deng, J. Jiang, C. Wang, *Sci. Adv.* **2018**, *4*, eaau9245.
[3] X. Fan, L. Chen, X. Ji, T. Deng, S. Hou, J. Chen, J. Zheng, F. Wang, J. Jiang, K. Xu, *Chem* **2018**, *4*, 174.
[4] S. Chen, J. Zheng, D. Mei, K. S. Han, M. H. Engelhard, W. Zhao, W. Xu, J. Liu, J. Zhang, *Adv. Mater.* **2018**, *30*, 1706102.
[5] J. Qian, W. A. Henderson, W. Xu, P. Bhattacharya, M. Engelhard, O. Borodin, J.-G. Zhang, *Nat. Commun.* **2015**, *6*, 6362.
[6] X. Ren, S. Chen, H. Lee, D. Mei, M. H. Engelhard, S. D. Burton, W. Zhao, J. Zheng, Q. Li, M. S. Ding, *Chem* **2018**, *4*, 1877.
[7] Z. Yu, P. E. Rudnicki, Z. Zhang, Z. Huang, H. Celik, S. T. Oyakhire, Y. Chen, X. Kong, S. C. Kim, X. Xiao, *Nat. Energy* **2022**, *7*, 94.
[8] Z. Yu, H. Wang, X. Kong, W. Huang, Y. Tsao, D. G. Mackanic, K. Wang, X. Wang, W. Huang, S. Choudhury, *Nat. Energy* **2020**, *5*, 526.
[9] Q.-K. Zhang, X.-Q. Zhang, H. Yuan, J.-Q. Huang, *Small Sci.* **2021**, *1*, 2100058.
[10] A. Watarai, K. Kubota, M. Yamagata, T. Goto, T. Nohira, R. Hagiwara, K. Ui, N. Kumagai, *J. Power Sources* **2008**, *183*, 724.
[11] C. A. Angell, in *Molten Salts from Fundamentals to Applications*, (Ed. M. Gaune-Escard) Springer, Dordrecht **2002**, pp. 305.
[12] F. Xu, C. Liu, W. Feng, J. Nie, H. Li, X. Huang, Z. Zhou, *Electrochim. Acta* **2014**, *135*, 217.
[13] S. Zhang, W.-J. Li, S.-G. Ling, H. Li, Z.-B. Zhou, L.-Q. Chen, *Chinese Phys. B* **2015**, *24*, 078201.
[14] K. Kubota, H. Matsumoto, *J. Electrochem. Soc.* **2014**, *161*, A902.
[15] K. Kubota, T. Nohira, R. Hagiwara, *J. Chem. Eng. Data* **2010**, *55*, 3142.
[16] R. Hagiwara, K. Tamaki, K. Kubota, T. Goto, T. Nohira, *J. Chem. Eng. Data* **2008**, *53*, 355.
[17] D. R. Wright, N. Garcia-Araez, J. R. Owen, *Energy Procedia* **2018**, *151*, 174.
[18] X. Lin, M. Salari, L. M. R. Arava, P. M. Ajayan, M. W. Grinstaff, *Chem. Soc. Rev.* **2016**, *45*, 5848.
[19] N. Plylahan, M. Kerner, D.-H. Lim, A. Matic, P. Johansson, *Electrochim. Acta* **2016**, *216*, 24.
[20] Z. Rao, S. Wang, *Renew Sustain Energy Rev* **2011**, *15*, 4554.
[21] K. Yan, J. Wang, S. Zhao, D. Zhou, B. Sun, Y. Cui, G. Wang, *Angew. Chemie* **2019**, *131*, 11486.
[22] J. Wang, W. Huang, A. Pei, Y. Li, F. Shi, X. Yu, Y. Cui, *Nat. Energy* **2019**, *4*, 664.
[23] F. Yonemoto, A. Nishimura, M. Motoyama, N. Tsuchimine, S. Kobayashi, Y. Iriyama, *J. Power Sources* **2017**, *343*, 207.
[24] M. Moreno, E. Simonetti, G. B. Appetecchi, M. Carewska, M. Montanino, G.-T. Kim, N. Loeffler, S. Passerini, *J. Electrochem. Soc.* **2016**, *164*, A6026.
[25] M. Kerner, N. Plylahan, J. Scheers, P. Johansson, *Phys. Chem. Chem. Phys.* **2015**, *17*, 19569.
[26] K. Kubota, T. Nohira, R. Hagiwara, *J. Chem. Eng. Data* **2010**, *55*, 2546.
[27] G. J. Janz, U. Krebs, H. F. Siegenthaler, R. P. T. Tomkins, *J. Phys. Chem. Ref. Data* **1972**, *1*, 581.
[28] P. G. Bruce, C. A. Vincent, *J. Electroanal. Chem. Interfacial Electrochem.* **1987**, *225*, 1.
[29] K. Kubota, T. Nohira, R. Hagiwara, *Electrochim. Acta* **2012**, *66*, 320.
[30] Z. Geng, J. Lu, Q. Li, J. Qiu, Y. Wang, J. Peng, J. Huang, W. Li, X. Yu, H. Li, *Energy Storage Mater.* **2019**, *23*, 646.
[31] X. Fan, L. Chen, O. Borodin, X. Ji, J. Chen, S. Hou, T. Deng, J. Zheng, C. Yang, S.-C. Liou, *Nat. Nanotechnol.* **2018**, *13*, 715.
[32] X. Cao, X. Ren, L. Zou, M. H. Engelhard, W. Huang, H. Wang, B. E. Matthews, H. Lee, C. Niu, B. W. Arey, *Nat. Energy* **2019**, *4*, 796.
[33] L. Su, A. Manthiram, *S.Struct.* **2022**, *3*, 2200114.
[34] Y. Liu, X. Tao, Y. Wang, C. Jiang, C. Ma, O. Sheng, G. Lu, X. W. Lou, *Science.* **2022**, *375*, 739.
[35] J. Chen, Q. Li, T. P. Pollard, X. Fan, O. Borodin, C. Wang, *Mater. Today* **2020**, *39*, 118.
[36] W. Xue, Z. Shi, M. Huang, S. Feng, C. Wang, F. Wang, J. Lopez, B. Qiao, G. Xu, W. Zhang, *Energy Environ. Sci.* **2020**, *13*, 212.
[37] F. Ding, W. Xu, G. L. Graff, J. Zhang, M. L. Sushko, X. Chen, Y. Shao, M. H. Engelhard, Z. Nie, J. Xiao, *J. Am. Chem. Soc.* **2013**, *135*, 4450.
[38] S. Hou, X. Ji, K. Gaskell, P. Wang, L. Wang, J. Xu, R. Sun, O. Borodin, C. Wang, *Science.* **2021**, *374*, 172.
[39] M. Schmidt, U. Heider, A. Kuehner, R. Oesten, M. Jungnitz, N. Ignat'Ev, P. Sartori, *J. Power Sources* **2001**, *97*, 557.